Proceedings of the Project Review, Geo-Mathematical Imaging Group (Purdue University, West Lafayette IN), Vol. 1 (2011) pp. 267-274.

ELASTIC FILMS AND REVERSIBILITY IN A MICROFLUIDIC PORE

YIHONG LIU*, DAVID NOLTE†, AND LAURA J. PYRAK-NOLTE‡

Abstract. Thin films of water in a single pore act as elastic membranes under tension that increase capillary pressures without increasing the dissipated mechanical work. A single wedge-shaped microfluidic pore was fabricated using two-photon laser machining of the photoresist SU-8 to have sharp corners at the pore entrance from the non-wetting reservoir. The singular geometry acts as a strong pinning defect that nucleates wetting films during drainage. The films are measured using confocal fluorescent microscopy on the transparent micromodel. The tension in the film behaves like an elastic tether that rigidly shifts the P_c-S_w scanning loop higher in pressure, while approximately conserving the dissipated mechanical work around the loop. This contribution of elastic forces to hysteretic dissipation has important consequences for the interpretation of P_c-S_w measurements in porous media.

1. Introduction. The physics of partially saturated porous media is controlled by the complex geometry and forces of the internal interfaces between the solid and the fluid phases. Interfaces in the Earth and laboratory are rarely in thermodynamic equilibrium, but they are often in metastable mechanical equilibrium characterized by the presence of films. Fluid films occur under many different conditions in the Earth. For example, partial melting along grain boundaries in ultramafic material results in the formation of melt films (Waff and Faul, 1992; Wirth, 1996). Water films beneath glaciers transport fine rock fragments through films that are only a few microns (micrometers) thick (Hallet, 1979, Iverson et al., 2003). Films provide a sustainable supply of water that participates in the ice fracturing of rock (Hallet, 2006). Water films are also thought to sustain microbial life in dry climes (Cary et al. , 2010) and deep in the Earth, and films participate in the recovery of oil and gas from subsurface reservoirs (Tchoukov et al, 2010).

In hydrology, films play a central role in many problems of multiphase flow in porous media, such as transport of colloids in subsurface environments [Wan and Tokunaga, 1997], support of microbial life [Or et al., 2007] and hydraulic conductivity in partially-saturated porous media [Beven and Germann, 1981; Germann, 1990; Tokunaga and Wan, 1997; Tuller and Or, 2001]. Hydraulic properties of water in soil and rock are central to our environment. For instance, to improve conceptual models for unsaturated hydraulic conductivity, a model has been proposed that considers pore-scale film and corner flow regimes in angular pore space [Tuller and Or, 2001; 2002; Tuller, et al., 1999]. In addition, film effects are a major transport mechanism in drying of porous media [Yiotis, et al., 2004].

The hysteresis of measured capillary pressure vs. saturation plays the central role in the characterization of porous media. Many theories seek to predict the magnitude of the hysteresis, and many upscaling approaches seek to extrapolate pressure-saturation curves from the laboratory to the field scale, and ultimately to predict fluid distributions in reservoirs. In our previous work (Liu, 2010; Liu et al., 2011), we demonstrated experimentally that the observed hysteresis in the capillary-pressure—saturation relationship for a single pore throat is defined by dissipative surface adsorption chemistry as the triple line moves during imbibition and drainage. The existence of hysteresis in a single pore provides the basic element for more complicated networks of pores with more complicated geometeries. However, the crucial role played by films was excluded from that study. In this paper, we nucleate films that are strongly pinned and observe a reversible shift in the P_c-S_w hysteresis that is consistent with an elastic restoring force. The effect on the capillary pressure is relatively large, but the closed-loop mechanical dissipation is surprisingly unaffected. These findings have important consequences in the interpretation P_c-S_w curves of complex porous media.

*Department of Physics, Purdue University, West Lafayette, IN, USA, Deceased

†Department of Physics, Purdue University, West Lafayette, IN, USA

‡Department of Physics, Purdue University, West Lafayette, Indiana, USA, and Department of Earth and Atmospheric Physics, Purdue University, West Lafayette, Indiana, USA and School of Civil Engineering, Purdue University, West Lafayette, Indiana, USA

2. Experimental Set-up. A single pore throat was fabricated in photoresist (SU-8) using two-photon polymerization to study the effect of films on the capillary-pressure—saturation relationship. An all-SU-8 wedge-shaped channel was fabricated using three stages of photolithography: contact lithography, broad-area exposure, and two-photon absorption. These created a single pore throat with uniform surface properties on all of the pore surfaces. Previous micro-model studies on pore-scale fluids had pore structures with walls of photoresist but floors and ceilings of glass distributions (e.g., Cheng et al., 2004, Chen et al, 2007, Pyrak-Nolte et al., 2008) or glass ceiling with all other walls in silicon (e.g., Keller et al., 1997; Baumann & Wirth, 2004; Grate et al. 2010).

In this study, an all-photoresist (SU-8) pore was created by coating the top and bottom glass cover slips (18 x 18 mm^2) with a 5 micron layer of SU-8, processing it and then performing broad-area exposure with UV (ultraviolet) light to photopolymerize the photoresist. On the lower cover slip, a second layer of SU-8 was spun to create a layer with a thickness of 40 microns. After soft-baking, the two-photon polymerization method (Liu et al., 2010a&b) was used to write the walls of the channels. Following the two-photon exposure, UV broad illumination was used to fabricate the 3 mm x 3 mm inlet and outlet ports, and a 900 μm long channel connecting the two ports. After processing, the sample was sealed by soft-baking on a hot plate at 65 °C and 95 °C for 1 min and 3 min, respectively. The entire micro-model was then exposed by a UV lamp for 10 sec and post-baked on a hot plate to crosslink the top layer. A full description of the fabrication technique can be found in Liu (2010) and Liu et al. (2011).

In the experiments, the micro-models were initially saturated with the wetting phase, i.e., water dyed with Alex-Fluor 488 at 1 mg / 10 ml. Lui et al. (2011) found that Alexa-fluor 488 reduced the surface tension of the dyed deionized water by only 0.25 mN/m (or 0.35%). Drainage and imbibition scans were performed by increasing and decreasing the non-wetting phase (air) pressures. As the air pressure increased, the wetting phase was displaced by the non-wetting. During each loop, the air pressure was varied in increments of 70 to 280 Pa/step while the water pressure was held constant. At each pressure step, a Laser Confocal microscope (Zeiss LSM 710) was used to collect a stack of confocal images over the depth of the channel. The confocal stacks were used to reconstruct the three-dimensional geometry of the fluid-fluid interfaces, fluid-solid interfaces, as well as the film structure. In our images, the transverse resolution is 1.19 µm/pixel and 0.714 µm/slice longitudinally. After each pressure increment, at least 5 minutes elapsed to establish mechanical equilibrium of the interface, and each confocal scan took about 1.5 minutes to complete for 85 z-scan frames. This same procedure was used for all imbibition and drainage scans.

To compare the P_c - S_w hysteresis with and without films, two types of scan loop were performed. First, the micro-model was saturated with the wetting phase to a saturation of $S_w \sim 0.95$ to avoid the generation of wetting films and to prohibit breakthrough of the wetting phase into the nonwetting-phase reservoir. Then, the air pressure was increased, (incrementally as described above) until a saturation of $S_w \sim 0.05$ was reached. After the drainage scan, the wetting phase was invaded, incrementally, into the throat until $S_w \sim 0.95$.

After collecting the drainage and imbibition scans for the system without films, the wetting phase was allowed to breakthrough past the non-wetting-phase outlet where a sharp edge in the fabricated micromodel nucleated film generation during the subsequent drainage. Films were observed to occur whenever the wetting phase passed the corners of the channel (S_w slightly greater than 1.0). The wetting phase was withdrawn from $S_w \sim 1.0$ to a saturation of 0.03, and was then invaded back to $S_w \sim 1.0$.

3. Results. The capillary pressure – saturation relationship for a single pore throat with and without films were determined from the measured capillary pressure, $P_{c,}$ and wetting phase saturation, - S_w, obtained from image analysis of the confocal stacks at each pressure. A comparison of the P_c - S_w relationship with (red curves) and without films (blue curves) is shown in Figures 1a & 1b for samples S5 and S7. When films are present, the capillary pressure is greater than in the no film condition. The capillary pressure for drainage increased between 500 $\sim$ 1000 Pa for $0.3 < Sw < 0.85$. At lower saturations the increase in capillary pressure was smaller and barely

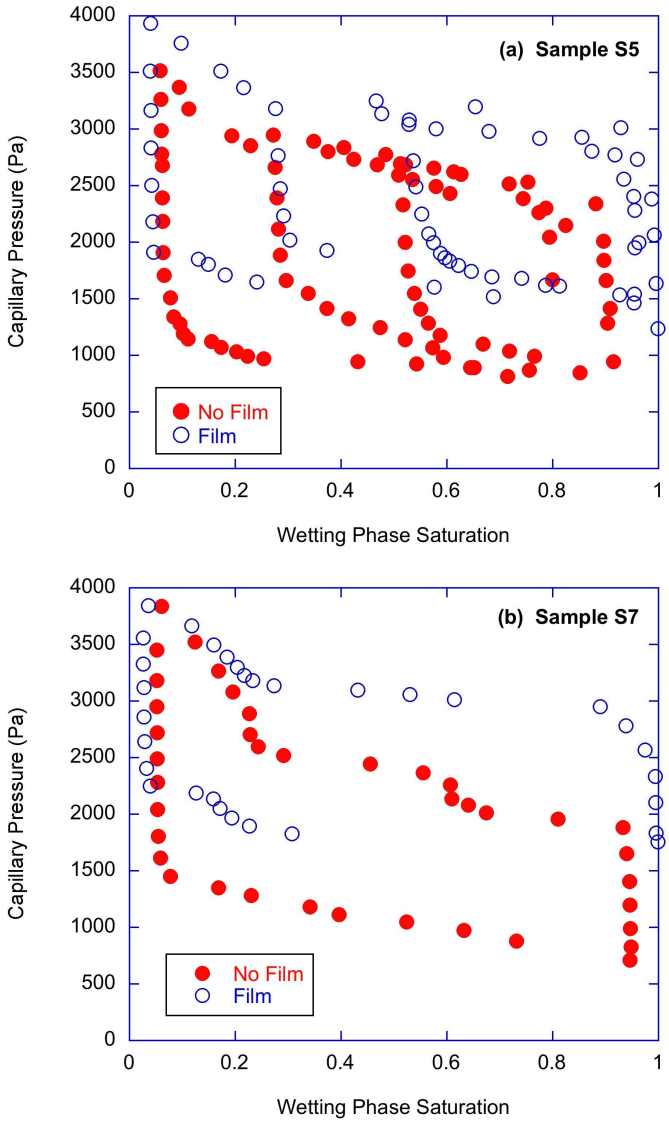

FIGURE 1. *Capillary pressure as a function of wetting phase saturation for (a) sample S5 and (b) sample S7 with and without films.*

observable $S_w < 0.1$. For imbibition, the increase in capillary pressure ranged between 600 – 900 Pa for $0.2 < Sw < 0.85$.

The presence of films also affected the contact angle between the wetting- nonwetting interface and the solid (Figure 2). The contact angles were extract from the confocal data both in the x-y and z-y planes. The contact angles as a function of wetting phase saturation or drainage and imbibition are shown in Figure 2 without films (red) and with films (blue). The contact angles exhibit hysteresis. The contact angle hysteresis is defined as $\Delta\theta = \theta_a - \theta_r$, where θ_a is the average advancing contact angle and θ_r is the average receding angle (Table 3.1.). When films are present, the advancing and receding contact angles are lower than those measured for the film case. This arises because the film exerts an additional force on the interface. The additional tension caused by the film distorts the interface thus reducing the contact angle. The film forces have the same direction during imbibition and drainage, though the displacements are in opposite directions.

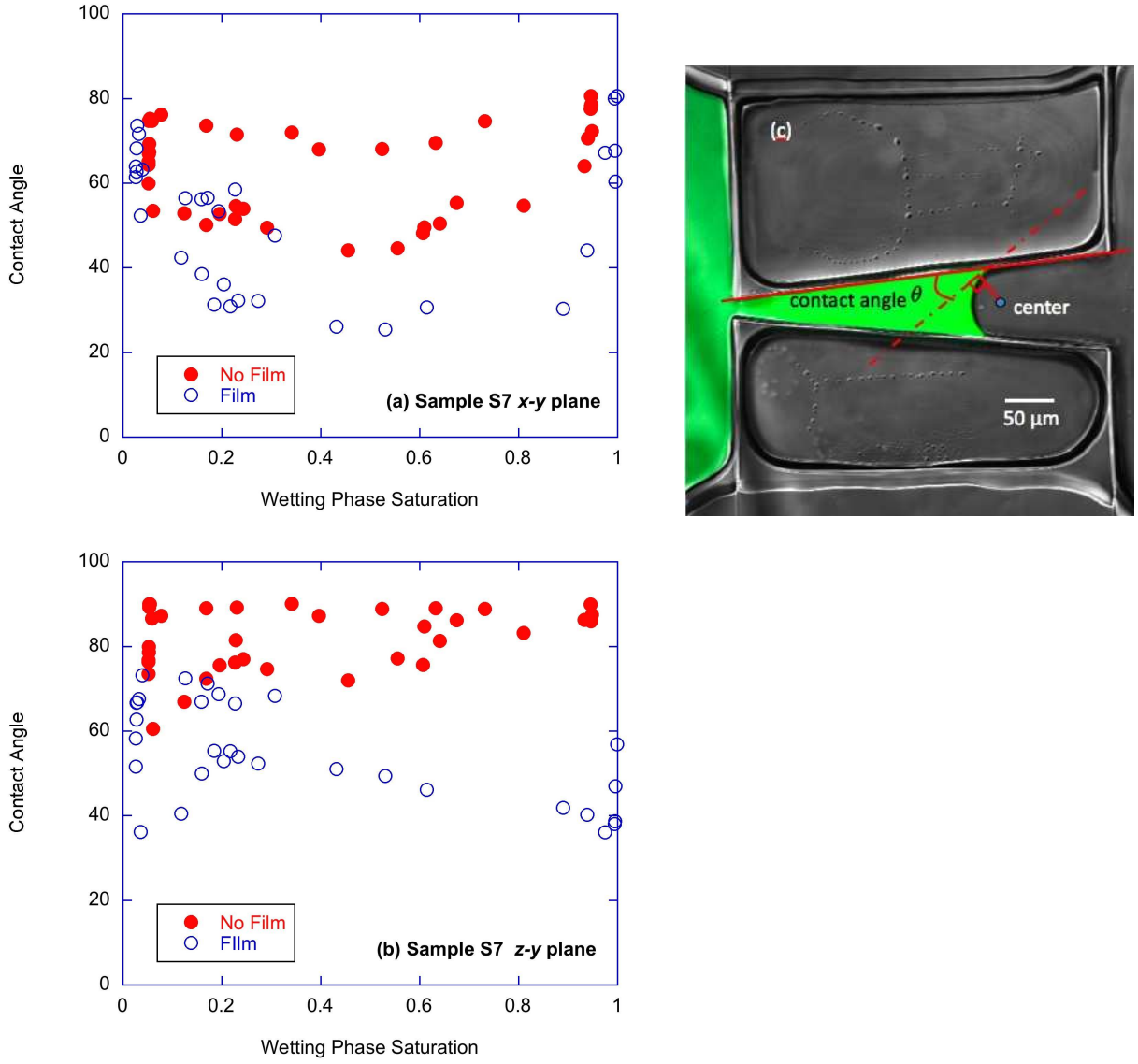

FIGURE 2. *The contact angles with and without films for sample S7 in the (a) x-y plane and (b) z-y plane. (c) Contact angle definition used in this paper.*

	θ_r Drainage	θ_a Imbibition	$\Delta\theta$ Hysteresis
No Film			
x-y	45°	70°	25°
z-y	70°	87°	17°
Film			
x-y	30°	55°	25°
z-y	50°	70°	20°

TABLE 3.1
Mean value of advancing and receding contact angles, and contact angle hysteresis

4. Analysis and Discussion. The hysteretic dependence of the capillary pressure (P_c) on the volume saturation of the wetting phase (S_w) depends on advancing and receding contact angles. When films are trapped along the channel, higher capillary pressure is required to drain the wetting phase than when there are no films. Thus, the film exerts an additional force against the withdrawal of wetting phase during drainage. Conversely, the film exerts a force that draws in the wetting phase during imbibition. Therefore, the force of the wetting-phase film to the wetting–non-wetting interface was always towards the non-wetting phase side. An estimation of the additional tension from the film is calculated from the tension balance

$$\begin{aligned} \sigma_{wn}\cos\theta_{nf} &= \sigma_{sn} - \sigma_{sw} \\ \sigma_{wn}\cos\theta_{f} &= \sigma_{sn} - \sigma_{sw} + \sigma_{film} \\ \hline \sigma_{wn}(\cos\theta_f - \cos\theta_{nf}) &= \sigma_{film} \end{aligned} \tag{4.1}$$

where σ_{wn}, σ_{sn}, σ_{ws} and σ_{film} are the surface tensions between the wetting and non-wetting phases, the solid and the non-wetting phase, the wetting phase and the solid, and for the additional tension provided by the film, respectively. In equation (4.1), θ_f and θ_{nf} represent the contact angle for the film and no film condition. Using equations (4.1), the film tension during drainage is approximately $0.112\sigma_{wn}$, or 0.0082 N/m, and during imbibition $0.126\sigma_{wn}$, or 0.0092 N/m.

To determine if this extra film force is conservative or dissipative, we compared the external work needed to the move the interface to the surface free energy. The external work ΔW is calculated from the area under the P_c – S_w curve by,

$$\Delta W = (P_w - P_n)\Delta V_w = -P_c V_{ch}\Delta S_w \tag{4.2}$$

and the free energy ΔF was calculated from the change in the surface areas ΔA_{ws} and ΔA_{wn}. The surface free energy is the sum of the interfacial tensions times the respective areas:

$$F = \Sigma\sigma_i A_i = \sigma_{wn}\Delta A_{wn} + \sigma_{sw}\Delta A_{sw} + \sigma_{sn}\Delta A_{sn} \tag{4.3}$$

Using $\Delta A_{sw} = -\Delta A_{sn}$ and $\sigma_{wn}\cos\theta_{a,r} = \sigma_{sn} - \sigma_{sw}$ in Equation 4.3 yields the change in surface free energy

$$\Delta F = \sigma_{wn}\Delta A_{wn} + \sigma_{wn}\cos\theta_{a,r}\Delta A_{sn} \tag{4.4}$$

Using this method, we calculated ΔW and ΔF based on the data sample from S7 and presented in Figure 3a). We find that both with and without the presence of film, the work required to move the interface equals the change in interface free energy, independently of the presence of films. This balance between surface free energy and work is a necessary condition from energy conservation, and the results verify this equality within experimental uncertainty (5%).

On the other hand, mechanical work is expended during imbibition and drainage caused by the irreversible movement of the triple line across the surface. The amount of dissipated mechanical work is equal to the area enclosed by a loop on the pressure-saturation plane. One of the chief questions we seek to answer in this paper is whether the presence of wetting films alters the amount of work. The areas enclosed by the P-S loops for the data in Fig. 1b (equal to the mechanical work performed around each loop) were 1.6 nJ (no film) and 1.4 nJ (film). The work is nearly equal with and without films, showing an energy balance in which the films act as an approximately conservative elastic force that shift the pressure-saturation loops to higher pressures, but do not significantly alter the enclosed work.

There is a 12% smaller hysteresis (work) for the case with films relative to without. The origin of the smaller dissipation for the film case can be found in the forces exerted by the film on the interface. The magnitude of the force from the films was calculated using

$$F = \Delta P_c \cdot A_{cs} \tag{4.5}$$

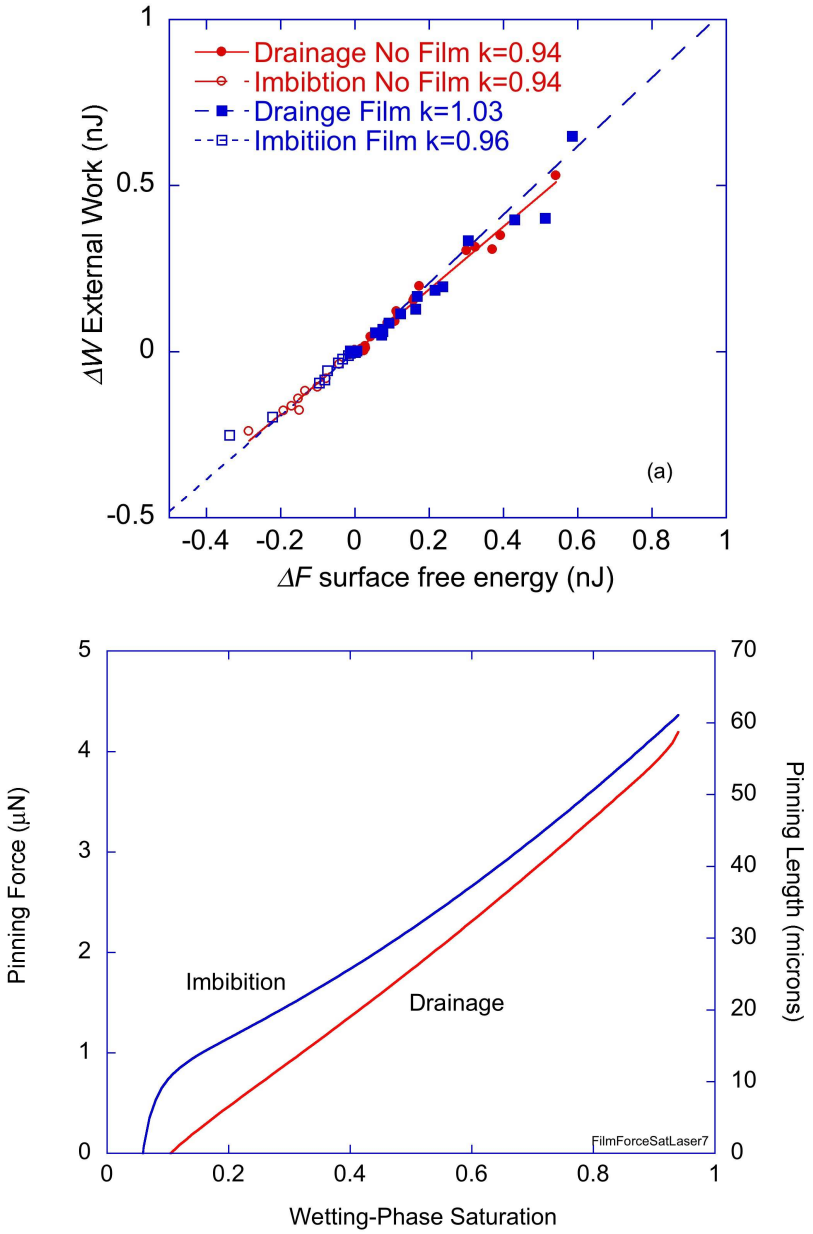

FIGURE 3. *(a) The external work as a function of surface free energy with (blue) and without films (red). "k" is the slope of the line. (b) The additional force by films during drainage as a function of wetting phase saturation.*

where F is the force from the films, ΔP_c is the pressure difference between drainage loops with and without film, and A_{cs} is the cross-sectional area of the channel. The film forces during drainage and imbibition are shown in Fig. 3b as functions of wetting-phase saturation. In each case the sample was initially saturated, then drained and imbibed. The pinning force is the force exerted by the films on the pinned length of the triple line at the sharp edge. At high saturation, the pinned length (obtained by dividing the pinning force by the surface tension of water in air) is nearly equal to twice the sample height of 40 microns, which is expected for two edges on each side of the nonwetting reservoir. The film force and pinning length decrease nearly linearly with decreasing wetting phase

saturation during drainage. In the subsequent imbibition, there is nearly a step function increase in the pinning force above the drainage value, followed by a nearly linearly increase with increasing saturation. This excess force during imbibition leads to positive work performed on the interface that is about 12% larger than drainage, in agreement with the work enclosed by the loop in the hysteresis.

Energy dissipation, during movement of the triple line, is the origin of hysteresis. The smaller hysteresis for the case with films is because the triple lines of the pinned films do not drag along the interface to the same degree as in the non-pinned case. Hence smaller areas swept out by the triple line in the case with films leads to smaller hysteresis. The surprising aspect of these results is that the presence of wetting films, which are metastable configurations and should exhibit irreversible relaxation towards equilibrium, actually reduced the amount of dissipation rather than increasing it. An important aspect of this conclusion is the time it takes for a single experimental loop, which is approximately 6 hours. The results suggest that the metastable films do not relax significantly in this time frame, which is in agreement with work by Liu et al (2011) who showed that, without films, there was small and extremely slow relaxation of interfaces in the micro-models. We performed independent relaxation experiments in the case with films, and although the relaxation was found to be larger and faster than without films, the relaxation was still small (a change of only 0.08 in saturation) over 5 hours. Therefore, the pinning of the triple line is extremely robust in these experiments.

5. Conclusions. In conclusion, we have performed a detailed force and energy analysis of the movement of interfaces in a single pore during drainage and imbibition in the two cases in which wetting films are either nucleated or prevented during drainage. We find that the wetting films exert an elastic force that is nearly conservative and reversible (within 12%) and that shift the hysteresis loops to higher pressure, but without significantly changing their enclosed areas. The experimental results are consistent with the conservation of total energy, and with mechanical work dissipated by sweeping the triple line across the sample surface. The wetting films in these experiments are strongly pinned and in metastable mechanical equilibrium, with negligible relaxation over many hours. The increase in measured capillary pressure has important consequences for the interpretation of field-data. Higher pressures measured in the field, or on laboratory core samples, would be interpreted as lower residual saturation, and hence higher production, but in fact the higher pressures may simply be going into elastic tension in films.

Acknowledgments. This research is supported by the National Science Foundation (0911284-EAR).

References.

1. Baumann, T. and C. J. Werth, Visualizaiton and modeling of polystyrol colloid transport in a silicon micromodel, Vadose, Zone Journal, 3: 434-443, 2003.
2. Beven, K., and P. Germann, Water-Flow in Soil Macropores .2. a Combined Flow Model, *Journal of Soil Science*, *32*, 15-29, 1981.
3. Cary, S. C., McDonald, I. R., Barrett, J. E. and D. A. Cowan, On the Rocks: The microbiology of Antarctic Dry Valley soils, Nature Reviews Microbiology, 8: 129-138, February 2010.
4. Chen, D. Q.,Pyrak-Nolte, L. J., Griffin, J. and N. J. Giordano, Measurement of interfacial area per volume for drainage and imbibition, *Water Resour. Res.,* 43, W12504, doi:10.1029/2007WR006021, 2007.
5. Cheng, J., Pyrak-Nolte, L. J., Nolte, , D. D. and N. J. Giordano, Linking pressure and saturation through interfacial areas in porous media, *Geophys. Res. Lett.,* 31, L08502, doi:10.1029/2003GL019282, 2004.
6. De Gennes, P.-G., Brochard-Wyart, F. and D. Quere, Capillarity and Wetting Phenomena, Drops, Bubbles, Pearls, Waves, Springer, New York, 2003.
7. Germann, P. F., Preferential Flow and the Generation of Runoff .1. Boundary-Layer Flow

Theory, *Water Resources Research*, *26*, 3055-3063, 1990.

8. Grate, J.W., Zhang, C., Wietsma, T. W. ,Warner,M. G. ,Anheier,N. C. ,Bernacki,B. E.,Orr,G.and M. Oostrom, A note on the visualization of wetting film structures and a nonwetting immiscible fluid in a pore network micromodel using a solvatochromic dye, *Water Resour. Res.,* 46, W11602, doi:10.1029/2010WR009419, 2010
9. Hallet, B., Why Do Freezing Rocks Break, Science, 314, 1092, DOI: 10.1126/science.1135200, 2006.
10. Iverson, N. R., Cohen, D., Hooyer, T. S., Fischer, U. H., Jackson, M., Moore, P. L., Lappegard, G. and J. Kohler, Effects of Basal Debris on Glacier Flow, Science, 301, 81, DOI: 10.1126/science.1083086, 2003.
11. Keller, A. A., Blunt, M. J. and P. V. Roberts, Micromodel observation of the role of oil layers in three-phase flow, Transport in Porous Media, 26: 277-297, 1997.
12. Liu, Y., Two-Photon Laser Fabrication of Large-Format Microporous Structures and the Study of Irreversible Microfluidic Processes, Ph.D. Thesis, Purdue University, West Lafayette, Indiana, 2010.
13. Liu, Y., Nolte, D.D. and L. J. Pyrak-Nolte, Hysteresis and interfacial energies in smooth-walled microfluidic channels, Water Resour. Res.*,* 47, W01504, doi:10.1029/2010WR009541, 2011.
14. Or, D., Smets, B.F. , Wraith, J.M. , Dechesne, A. and S.P. Friedman, Physical constraints affecting bacterial habitats and activity in unsaturated porous media – a review, Advances in Water Resources 30, 1505–1527, 2007.
15. Pyrak-Nolte, L. J., Nolte, D. D., Chen, D. and N. J. Giordano,Relating capillary pressure to interfacial areas, *Water Resour. Res.,* 44, W06408, doi:10.1029/2007WR006434, 2008.
16. Tchoukov, P., Czarnecki, J. and T. Dabros, Study of water-in-oil thin liquid films: Implication for the stability of petroleum emulsions, Colloids and Surfaces A: Physicochemical and Engineering Aspects, 372: 15-21, 2010.
17. Tokunaga, T. K., and J. M. Wan, Water film flow along fracture surfaces of porous rock, *Water Resources Research*, *33*, 1287-1295, 1997.
18. Tuller, M., et al., Adsorption and capillary condensation in porous media: Liquid retention and interfacial configurations in angular pores, *Water Resources Research*, *35*, 1949-1964, 1999.
19. Tuller, M., and D. Or, Hydraulic conductivity of variably saturated porous media: Film and corner flow in angular pore space, *Water Resources Research*, *37*, 1257-1276, 2001.
20. Tuller, M., and D. Or, Unsaturated Hydraulic Conductivity of Structured Porous Media: A Review of Liquid Configuration-Based Models, *Vadose Zone Journal*, *1*, 14-37, 2002.
21. Waff, H. S. and U. H. Faul, Effects of Crystalline Anistropy on Fluid Distribution in Ultramafic Melts, Journal of Geophysical Research, 97(B6): 9003-9014, June 10, 1992.
22. Wirth, R., Thin Amorphous films (1-2 nm) at olivine grain boundaries in matle xenoliths from San Carlos, Arizona, Contrib. Mineral Petrol. 124: 44-454, 1996.
23. Yiotis, A. G., et al., Effect of liquid films on the drying of porous media, *Aiche J.*, *50*, 2721-2737, 2004.